Chapter 9 Electrochromic Windows with Multi-layer Structures

9.1. Electrochromic Windows

9.1.1. Basic working principle of the WO_3 electrodes

When a voltage is applied on ECDs or EC windows (Fig. 1-1, Chapter 1), ions are inserted into the WO_3 film in the device, whose optical properties thereby are changed. It switches reversibly from transparent to dark blue upon electrochemical redox reactions. The believed mechanism of ECDs still remains unclearly explained, but on the basis of the present knowledge we give a summary of it as follows.

The insertion/extraction process can be represented by:

WO_3 (transparent) + xLi^+ (or H, Na, K) + xe^- $\Leftrightarrow$ Li_xWO_3 (blue).

This reaction goes to the left or right depending on the sign of the applied voltage. When ions are inserted, both XPS [1] and electron spin resonance (ESR) [2] show that W^{5+} as well as W^{6+} are present, and that the W^{5+} density scales with the intensity of the EC absorption peak. They can also be explained in other ways.

(I) By an intervalence charge-transfer transition (ICTT): $W^{5+}{}_A + W^{6+}{}_B + h\nu \Leftrightarrow W^{6+}{}_A + W^{5+}{}_B$, where A and B denote adjacent tungsten ions. The injected electrons are localized on tungsten ions and the charge transfer between tungsten ions caused absorption of the film.

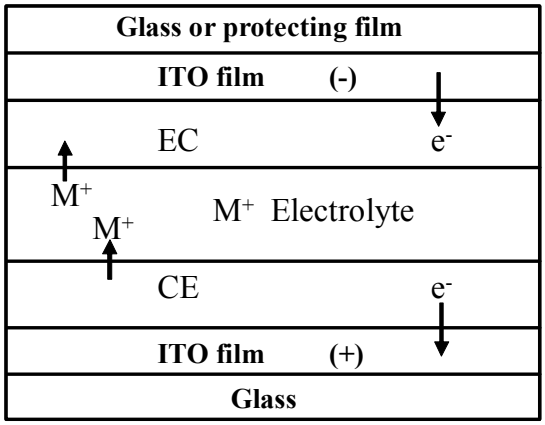

Fig. 9-1. Schematic structure of the electrochromic process in electrochromic (EC) windows. It consists of thin EC and counter electrode (CE) coatings that are sandwiched between the two ITO films.

(II) By Deb's first colour-centre model: oxygen vacancies with one trapped electron causes the coloration [3].

(III) By the presented W^{5+} ions which are localized in distorted octahedrals of the film.

Fig. 9-1 shows the schematic structure of the electrochromic process. It consists of a thin EC and a counter electrode (CE) coating that is sandwiched between two ITO films. Ion (M^+) conducting and electron (e^-) blocking electrolyte film separates EC and CE films.

9.1.2. Electronic and ionic conduction of WO_3 film

As described in section 7.1 (Chapter 7), one of the structural peculiarity-features of tungsten trioxide, related to non-stoichiometry, is a variety of phases based on [WO_6]-octahedron sharing in the structural units of pure tungsten oxide compounds with crystalline patterns (oxygen based non-stoichiometry). Another basic common peculiarity-feature of tungsten trioxide phases is the ion insertion or extraction phenomenon (ion insertion based non-stoichiometry). The pure tungsten oxide compounds are quasi electronic conductors, and they are also ion conductors because of the ion insertion or extraction phenomenon. The non-stoichiometry influences the formation of particles of tungsten oxide compounds during the thin film deposition.

The sharing types (corners, edges, planes) of [WO_6]-octahedron, and the structure of the different non-stoichiometric phases depend on oxygen deficiency. It plays the main role for obtaining α-WO_3 films whose constitution is based on nano-size particles with long-range order. The surface of all these compounds has a high adsorption capability for different chemical species and a high catalytic activity. This is due to the above descriptive non-stoichiometry and concerns the composition, constitution and structure of the film. The porous thin films with polycrystalline or amorphous structure (heterogeneous systems with developed inner surface and adsorbed chemical substances) can be obtained by PVD (Physical vapor deposition) technique. The conductivity can be changed by ion insertion / extraction or redox reactions.

The adsorbed gases and water in pores on the surface of the oxide form different interfaces. The hydration level of WO_3 films is more or less constant for substrate temperature up to 200 ^{0} C, during the deposition of the films. Above 200 ^{0} C electronic conduction dominates. Adsorbed water serves as a source of hydrogen ions (protons). Any adsorbed chemical compound interacts with electronic and ionic defects on nano-

sized crystal particles. It changes the conductivity of the oxide phase. The boundary between adsorbed water (liquid phase) – oxide (solid phase) can interact with a gas phase too. For investigation of poly-chromic phenomena in WO_3 films such assumptions are very important. The WO_3-film boundary with the electrode is a more complicated case: in the electrode processes three (electrode - metal layer, oxide and water or gas) and four (electrode - metal layer, oxide, water and gas) phases can be involved. The colour centers, for example, can be induced thermally (increase of non-stoichiometry) or electrically (injected ions). The poly-chromism of α-WO_3 films can be directly related to ion insertion/extraction processes. These processes or solid state redox reactions in α-WO_3 films are sensitive to external forces which induce reversible optical effects.

9.1.3. Calculation of structural data and possibility of ion movement

Intercalation of Li, H, or Na in WO_3 leads to intricate structural changes that are not yet fully understood. However we can explain why the EC behavior of a α-WO_3 film is better than that of a crystalline WO_3 film. The average atomic radius (empirical) of K, Na, Li and H are ~0.220 nm, ~0.180 nm, ~0.167 nm and ~0.037 nm respectively [4]. The average size of a tunnel of three member ring, six member ring and monoclinic WO_3 structure are ~0.26 nm, ~0.52 nm and ~0.30 nm respectively, calculated from the structure data (Section 7.2.3) and Fig 7-2-1b and 7-2-3ab. The size of H^+ is ~0.074 nm, so H^+ can go through all 3 kinds of tunnels during the insertion; however it is not used widely due to its unstable EC property. The size of Li^+ (Na^+) is ~0.33 (0.36) nm, which means that these ions can only go through tunnels created by the six member ring.

9.2. Effect of the Structure on the Electrochromism of Tungsten Oxide Films

9.2.1. Introduction

C. G. Granqvist has reported that the coordination of the ions leads to electronic band structures that, at least for the defect perovskite and rutile lattices, can explain the presence or absence of cathodic and anodic electrochromism [5]. Generally it is thought that a loose packing allows small ion transport easily within the material. Specially, for a columnar structure the intercolumnar regions allow easy transport of ions across the film, which is important for the dynamics of EC windows. The transport mechanism can

be vehicular, Grotthuss-type, or a mixture of these [5]. However one can't explain how small ions move easily within a long-range crystallite.

Here we try to point out some fundamental microstructures of the WO_3 material and explain that these microstructures are of decisive importance for the electrochromism. We show how the microstructure allows the ions move and why sometimes the amorphous film has good electrochromism while the crystalline film has not good electrochromism or no electrochromism.

The ubiquitous octahedral building impedes the movement of the ions, if the size of tunnel is smaller than the size of the ions. Traditional amorphous or fine-grained tungsten oxygen films were considered to have good EC behavior, but this isn't right and there are problems in applications. In practice more well-crystallized films with larger grain sizes are required. The transmittance and reflectance of WO_3 films are strongly dependent on the crystallinity and grain size of the film [6]. It includes the intercalation state of ions such as Li^+, H^+ and K^+.

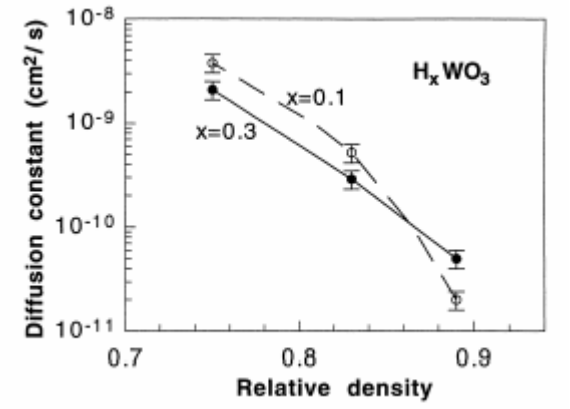

Fig. 9-2. Diffusion constants versus relative density for sputter deposited tungsten oxide films. Data are given for two levels of proton intercalation [7].

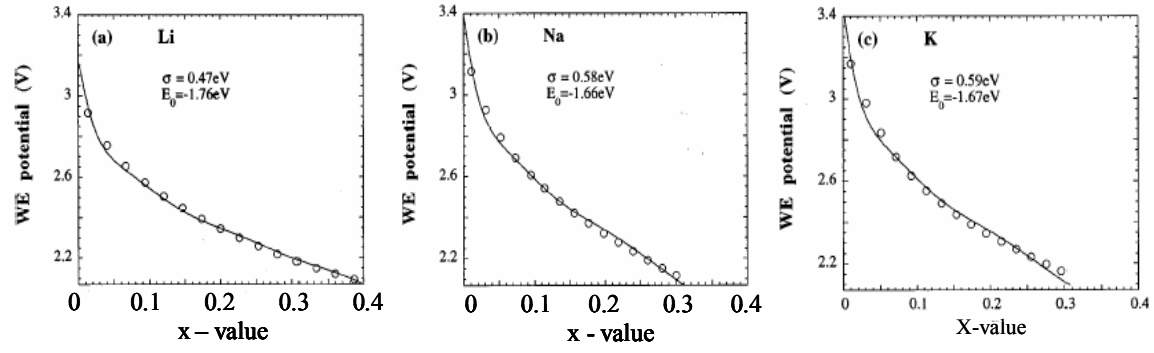

Fig. 9-3. Potential versus ionic content for sputter deposited tungsten oxide films containing Li(a), Na(b) and K(c). The data was measured in a three-electrode arrangement with the W oxide film as working electrode (WE) and Li foil as reference electrode [8].

9.2.2. Diffusion constant k_d

Ion intercalation de-intercalation governs the optical modulation in EC tungsten oxide. The diffusion constant k_d of the ionic species is an important parameter since it determines the dynamics of the optical change. Granqvist [5] and others concluded that the magnitude of k_d depends strongly on the porosity of the film. In fact this is not exact and bring some misguide. Wang et al [7] have reported data on proton diffusion versus relative density (D) of the tungsten oxide films prepared by magnetron sputtering at different plasma pressures (Fig. 9-2). From the figure, there is a turning point of relative density D_T (0.86). Clearly when $D < D_T$, Granqvist´s explanation or conclusion is right. The effect of increasing porosity is important to k_d of ions. The diffusion constant k_d decreases when protons content x is increased from 0.1 to 0.3 if the film is porous. However in crystalline film or compact films, the effect of x on k_d is the opposite. This phenomenon can be explained by the following "forced intercalation model".

9.2.3. Forced intercalation model

In fact the Li^+ ions can be insert not only into disordered perovskite structure films, but sometimes also into crystalline film, even if the size of the Li^+ ion is bigger than that of the tunnel in the film. This happens with the phenomena of strong external force (high potential or high energy), very slow response time, and irreversible cycle. All these can be explained by the change of the working electrode potential of the well-crystallized WO_3 films, in different ionic contents, to the different kind of ions such as Li (or Na, and K) in Fig. 9-3 [8]. The change of the voltage between the WO_3 film and the reference electrode reaches ~0.1 V. Clearly the potential decreased in a step-like manner as x goes from zero to 0.3 for the heavily intercalation. The atomic radius (weight) of K, Na and Li are 0.220 nm (39.098), 0.180 nm (22.990) and 0.167 nm (6.941) respectively. Even if they have clearly difference in the radius and weight, when the ionic intercalation content is fixed at a value, the external working electrode potential of Na and K is still similar. The external force- working electrode potential of Li is smaller than that of Na and K, because the size of Li^+ is much smaller than that of the six member ring (~0.52 nm, Section 9.1.3). This demonstrates and supports the proposed model and explanation. Other experiments have also shown the effect of non-reversible coloration by ion beam irradiation on tungsten oxide films [9]. The studies of various types of ions (^{2}He, ^{15}N, ^{16}O, ^{23}Na, ^{40}Ar, ^{70}Ga) with energies in the keV and MeV range were done.

9.3. Model of Electrochromism and Numerical Simulation

9.3.1. The physical model

The kinetics of electrochromism has been an important topic [10-13]. Here a model of the coloration and bleaching(C/B) process is proposed. It is recognized that the coloration process is based on double injection of ions and electrons forming the tungsten bronze M_yWO_3. Other possible effects such as a barrier at the counter electrode, a barrier at the electron-injecting contact, and charge transport in the electrolyte were considered to be neglectful.

A coloration model based on the condition of constant voltage was chosen. Generally the following factors limit coloration current in our model. (i) a barrier at the ion injecting interface (electrolyte/WO_3 interface); (ii) diffusion of ions within the electrochromic films; and (iii) the series resistance of the cell. Factor (i) is present at all times and it dominates the coloration dynamics at low voltages (< 5 Volts). This is in agreement with Luo *et al.*'s idea [11]. Factor (ii) is likely to be important at higher applied voltages (>5 Volts).

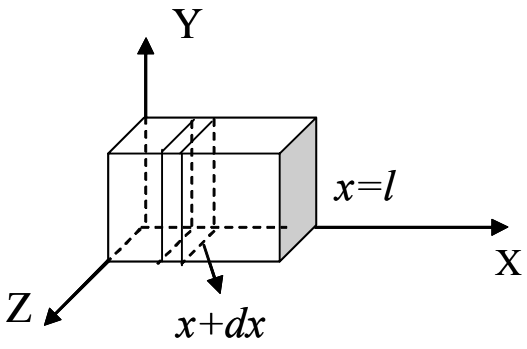

Fig. 9-4. The Li^+ motion in the film governed by diffusion processes was considered. The cross sections x remain plane with a certain ion concentration and parallel to each other during their displacement along the x axis of the plate.

9.3.2. Differential equation of the model

Let us consider a plate as an electrochromic film which has homogeneous diffusion of ions (such as Li^+). We shall deal with the plate to study the ions diffusion. We can consider the case of the diffusion of "foreign ions" denoting the corresponding diffusion coefficients as foreign diffusion coefficients. It is not self-diffusion. We shall also confine to diffusions in which the cross sections x remain plane and parallel to each

other during their displacement along the x axis of the plate (Fig. 9-4). The condition is justified if the plate and the applied electric field to the plate are homogeneous in the direction of y and z axis.

If two planes of the plate have somewhat different ion concentrations along its x axis, it will start diffusing under the applied electrical field. In order to study the diffusion processes one must establish a gradient of ion concentration. Let us assume that the initial state and the end state of the diffusion are at the points x=0 and x=l. Suppose that x is the abscissa of an arbitrary cross section in the plate. Let us denote by u (x, t) the displacement of this section at the time t. Then, the displacement of the section whose abscissa is x+dx will be equal to

$$u + \frac{\partial u}{\partial x} dx .$$

Thus, it is clear that the relative lengthening of the plate at the cross section whose abscissa is x is given by the derivative

$$\partial u(x,t) / \partial x.$$

Recalling that the diffusion undergoes only a small part of all the thickness of the plate (film), we can compute the ion diffusion flow q in this cross section. From experiments and Fick's first law [14], we have

$$q = -k_d \frac{\partial u}{\partial x}, \qquad (9.3.1)$$

where k_d is the diffusion coefficient of the ions in the film, and $\partial u(x,t) / \partial x$ is the gradient of ion concentration. The experimental measurement of k_d is surveyed in ref. [14]. Let us consider the element of the plate included between two cross sections whose abscissas, when the process is at the beginning, are x and x +dx. In the element it is considered that the ions move in q_x and out q_{x+dx} , which are directed along the x-axis. The values of the resultant of these ion movements in the time Δt are

$$[q_{x+dx} - q_x]S\Delta t = [(k_d \frac{\partial u}{\partial x})_{x+dx} - (k_d \frac{\partial u}{\partial x})_x]S\Delta t = k_d \frac{\partial^2 u}{\partial^2 x} \Delta x S \Delta t \qquad (9.3.2)$$

and are also directed along the x-axis, where S is the cross sectional area. On the other hand, the amount of these ions moving in is equal to the obtained amount of the ions in the element,

$$k_d \frac{\partial^2 u}{\partial^2 x} \Delta x S \Delta t = \Delta x S \Delta u \qquad (9.3.3)$$

so that we obtain the equation

$$\frac{\partial u}{\partial t} - k_d \frac{\partial^2 u(x,t)}{\partial x^2} = 0 \qquad (9.3.4)$$

9.3.3. Coloration process in the simulation model for ion injection

In order to determine the response in the use of constant charge injection, we start the diffusion Eq.(9.3.4) at some boundary conditions. Solving this equation by using Laplace transforms or Fourier method gives an expression for the concentration of injected ions $u(x, t)$ in the film as a function of the distance from the electrolyte/film interface (x), and the coloring time (t), as well as the relationship between the $u(x, t)$ and diffusion coefficient (k_d). From these results the variation of voltage or current versus time can be obtained. The ion concentration is expressed as follows.

$$u(x, t) = \sum_{n=1}^{\infty} [\frac{2}{l} \int_0^l \varphi(x) \sin \frac{n\pi x}{l} dx] e^{-(k_d)(n\pi/l)^2 t} \sin \frac{n\pi x}{l} \qquad (9.3.5)$$

The detail application of a Fourier method to the solution of boundary-value problems for the differential equation is presented in the following part.

9.3.4. The application of the Fourier method to the solution of boundary-value problems for the differential equation

Case I.

Consider a plate as an electrochromic film which has an homogeneous diffusion of ions like in Section 9.3.2, and the two sides are kept at zero concentration at an external electrical field. That is, Eq.(9.3.4) is subject to the boundary conditions at *x=0* (electrolyte/ EC film interface) and *x=l* (the EC film/conductor interface)

$$u|_{x=0}=0 \ , \ u|_{x=l}=0 \qquad (9.3.6)$$

and the initial condition

$$u|_{t=0}=\varphi(x), \qquad (9.3.7)$$

where φ (x) is continuous, has a piecewise-continuous derivative, and vanishes at *x=0* and *x=l*.

Following the Fourier method [15], we can look for solutions to Eq.(9.3.4) in the form

$$u(x, t) = X(x)T(t) \qquad (9.3.8)$$

Substituting Eq. (9.3.8) into Eq. (9.3.4), we have

$X(x)T'(t) = k_d T(t)X''(x)$ and then

$$\frac{T'(t)}{k_d T(t)} = \frac{X''(x)}{X(x)} = -C.$$

Two equations are obtained as follows,

$$T'(t) + k_d CT(t) = 0, \qquad (9.3.9)$$

$$X''(x) + C X(x) = 0 \qquad (9.3.10)$$

To obtain a non-trivial solution to Eq. (9.3.4) in the form Eq.(9.3.8) satisfying the boundary conditions Eq. (9.3.6), we need to find a non-trivial solution to Eq. (9.3.10) satisfying the boundary conditions

$$X(0) = 0, \quad X(l) = 0 \qquad (9.3.11)$$

Thus, to determine the function X(x), we are led to the eigenvalue problem [15]. It was shown there that only for values of the parameter C that are equal to

$$C_n = (n\pi/l)^2 \quad (n = 1, 2, 3, \ldots\ldots), \qquad (9.3.12)$$

are there non-trivial solutions to the problem (9.3.10):

$$X_n(x) = \sin\frac{n\pi x}{l}. \qquad (9.3.13)$$

The values $C = C_n$ correspond the solutions to Eq. (9.3.9):

$$T_n(t) = a_n e^{-(k_d)(n\pi/l)^2 t}, \qquad (9.3.14)$$

where a_n are arbitrary constants. Thus, all the functions

$$u_n(x, t) = X_n(x)T_n(t) = a_n e^{-(k_d)(n\pi/l)^2 t} \sin\frac{n\pi x}{l} \qquad (9.3.15)$$

satisfy Eq. (9.3.4) and the boundary conditions (9.3.6) for arbitrary values of the constants a_n.

Let us construct the series

$$u(x, t) = \sum_{n=1}^{\infty} a_n e^{-(k_d)(n\pi/l)^2 t} \sin\frac{n\pi x}{l} \qquad (9.3.16)$$

When we satisfy the initial condition (9.3.7), we obtain

$$u(x, 0) = \varphi(x) = \sum_{n=1}^{\infty} a_n \sin\frac{n\pi x}{l}. \qquad (9.3.17)$$

This series is an expansion of the function φ (x) in a Fourier sine series for the interval $(0, l)$. The coefficients a_n are determined from the familiar formula

$$a_n = \frac{2}{l}\int_0^l \varphi(x) \sin\frac{n\pi x}{l}\, dx. \qquad (9.3.18)$$

From the above we can show that the function u(x, t) has continuous derivatives of arbitrary order with respect to x and t in the region $0<x<l$, $t>0$.

Case II.

For another particular case, consider the boundary conditions at $x=0$ (electrolyte/the EC film interface) and $x=l$ (the EC film/conductor interface) which are kept at a constant concentration.

$u|_{x=0}$=C1=constant , $u|_{x=l}$=C2= constant

Similarly we obtain

$$u(x,t) = C1 + (C2-C1)\frac{x}{l} + \frac{2}{\pi}\sum_{n=1}^{\infty}\frac{(-1)^n C2 - C1}{n} e^{-(k_d)(n\pi/l)^2 t}\sin\frac{n\pi x}{l}$$

$$+\sum_{n=1}^{\infty}\left[\frac{2}{l}\int_0^l \varphi(x)\sin\frac{n\pi x}{l}\,dx\right]e^{-(k_d)(n\pi/l)^2 t}\sin\frac{n\pi x}{l} \qquad (10.3.19)$$

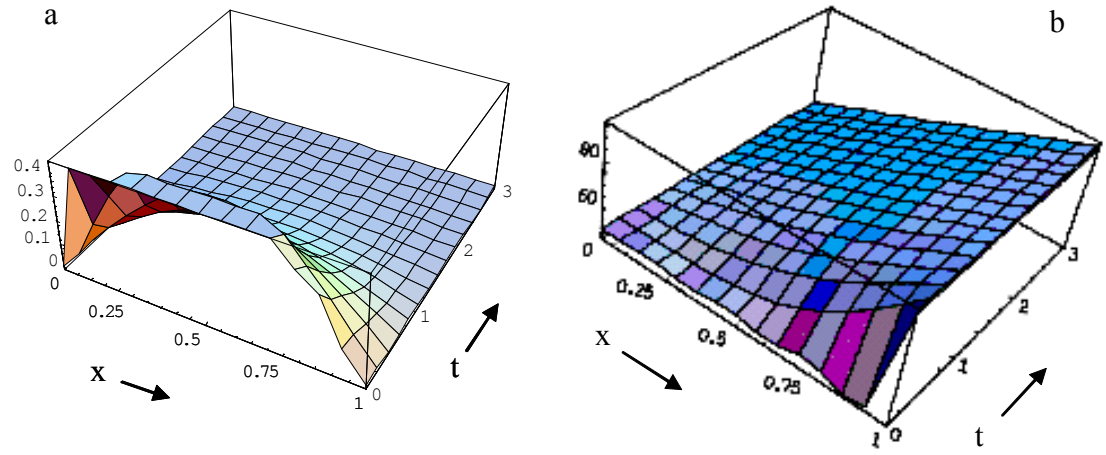

Fig. 9-5. The three dimensional (3D) curves of the distribution of ion concentration obtained by mathematical simulation. (a) representation of Eq. (9.3.5), (b) representation of Eq. (9.3.19).

In order to give a good understanding of the above models, simulations and results, the 3D curves of the distribution of ion concentration were plotted using the Mathematica-4.1 Software. The following two conditions were used as examples to give a physical meaning:

1. When the diffusion coefficient of Li^+ ion - k_d is 0.2 cm²/s, $u|_{x=0}$=0 (Li^+ ion concentration at one interface of WO_3/ITO), $u|_{x=l}$=0 (Li^+ ion concentration at counter interface of WO_3/ITO, the thickness of WO_3 film is l), l = 1cm, and $\varphi(x) = 1-x^2$ (one example of the distribution of resident Li^+ ion concentration inside WO_3 film at initial

time or before applying the electrical voltage.), the calculated results of Eq. (9.3.5) are shown in Fig. 9-5a.

2. The calculated results of Eq. (9.3.19), when k_d is 0.2, $u|_{x=0}$=C1=50, $u|_{x=l}$=C2=5, l = 1, and $\varphi(x) = 1-x^2$, are shown in Fig. 9-5b.

9.4. Electrochromic Devices

9.4.1. Solid state devices

Multilayer films based on tungsten oxide have been investigated by many researchers for future electrochromic windows, but in most cases the WO_3 films on ITO were cycled in either 1M lithium triflate in propylene carbonate or 1M H_2SO_4 or other solution electrolytes. Currently the ECD research is focused to develop solid-state devices from simulation study in three electrode electrochemical cells, half solid-state devices (using liquid electrolyte)[6, 16-17]. Recently, I. Porqueras and E. Bertran [18-19] investigated the properties of WO_3 films on insertion of lithium, combining the physical vapor deposition-"dry method" and three electrode electrochemical cells, for understanding the work and mechanisms of the solid ECDs. The appropriate configuration of an all solid-state ECD for window applications is a multi-layer film based on WO_3. A schematic representation of the ECD structure, that we assembled, composed on ITO/WO_3 / Li^+ solid-state electrolyte /ZrO_2 or SnO_2/ ITO. Our aim is to fabricate an all solid state EC devices. The solid state EC windows (or devices) were fabricated in this thesis work. The modulation was observed in the ECDs which were prepared.

9.4.2. Preparation of SnO_2 films and Mo (and Fe) doped SnO_2 films for counter electrode

Searching for new counter electrodes with high transmittance is important for ECDs. SnO_2 film is one of the transparent conductors that received significant commercialization. There are many reviews, preparations and characteristics in the literatures [20-22]. SnO_2 films are prepared through many industrial techniques like PVD, CVD, sol-gel, powder sintering, spray pyrolysis, and laser ablation [23]. It has a tetragonal lattice (a: 4.737 Å) and can be mono-crystalline or polycrystalline. Here the SnO_2 thin film is obtained by using reactive dc magnetron sputtering. This technique allows produce thin films with different structural and physical characteristics. The

influence of the deposition conditions on the microstructure and the properties of the SnO_2 films has been studied for different $P_{O2,}$ total sputtering pressures, substrate temperatures, substrate-target distances, and dc powers. Doping of SnO_2 with other metals (or its oxides) results in a larger grain size, in clear effects to the preferred orientation of crystallites and in different physical properties.

It is found that the SnO_2 is stabilized in multilayers in which its layer thickness is less than 500 nm. The deposition conditions of the SnO_2 films are shown in Table 9-1 to Table 9-3.

Table 9-1. The deposition conditions of the SnO_2 films with different Fe concentrations

No. of the samples	H1	H2	H3	H4	H5	H6	H7	H8	H9	H10	H11
P_{O2} (%)	75	45	35	30	30	30	60	30	30	60	45
Sputtering pressure(mbar)	3×10^{-2}										
dc power (W)	125										
Substrate Temperature (^{0}C)	Room temperature										
Base pressure (mbar)	1×10^{-5}										
P_{Ar} (10^{-2} mbar)	0.75	1.65	1.85	2.10	2.10	2.10	1.20	2.10	2.10	1.20	1.65
Deposition time (Min.)	30	40	50	30	30	30	30	30	50	60	50
Fe concentration (%)	0	0	0	0	1.01	1.01	1.01	1.52	1.52	1.52	1.52
Substrate-target distance (mm)	60	60	60	60	60	54	54	54	54	54	54

Table 9-2. The deposition conditions of the SnO_2 films with different Mo concentrations

No. of the samples	Y1	Y2	Y3	Y4	Y5	Y6	Y7	Y8	Y9	Y10	Y11
P_{O2} (%)	30%										
Sputtering pressure (mbar)	3×10^{-2}										
dc power (W)	125										
Substrate-target distance (mm)	60										
Base pressure (mbar)	1×10^{-5}										
P_{Ar} (mbar)	2.1×10^{-2}										
Deposition time (Min.)	50	50	50	50	50	50	50	50	50	50	50
Mo concentration (%)	0	1.9	3.1	4.0	5.1	6.0	6.8	7.9	9.1	10.0	10.0
Substrate temperature	RT	RT	RT	RT	RT	RT	RT	RT	RT	RT	300^{0}C

Table 9-3. The deposition conditions of the SnO_2 films prepared at different dc power

No. of the samples	N51	N52	N53
dc power (W)	105	115	125
Sputtering pressure (mbar)	3×10^{-2}		
P_{O2}	30%		
Substrate-target distance (mm)	60		
Temperature	Room temperature		
Sputtering time (Min.)	30	30	30

9.4.3. Preparation of ZrO_2 films for counter electrode

ZrO_2 films have many important applications, due to their optical properties (high refractive index, low absorption over a broad spectral region from the near-UV to mid-IR, high laser damage threshold), thermal properties (low thermal conductivity and high thermal expansion coefficient), high dielectric constant and corrosion-resistant properties. These films can be used as bond layers for optical coating [24-25], bond layer for thermal barrier coatings [26-28], buffer layer for $YBa_2Cu_3O_{7-x}$ thin films [29], dielectric films [30], and protective coatings [31]. In this work the objective is to study the influence of the ZrO_2 film, and its potential use as the ionic conducting or storage layer in solid-state EC devices. The ZrO_2 films prepared by the reactive magnetron sputtering technique have been studied. The influence of the deposition conditions on the microstructure and the properties of ZrO_2 films have been studied for different $P_{O2,}$ total sputtering pressures, substrate temperatures, substrate-target distances and dc powers. Some data of the deposition conditions are shown in Table 9-4 to Table 9-7.

Table 9-4. The deposition conditions of the ZrO_2 films prepared with different P_{O2}

No. of the samples	Z1	Z2	Z3	Z4	Z5	Z6	Z7	Z8	Z9
P_{O2} (%)	20	25	30	35	40	45	50	55	60
Sputtering pressure (mbar)	5×10^{-3}								
dc power (W)	85								
Substrate-target distance (mm)	60								
Substrate Temperature	Room temperature								

Sputtering time (Min.)	10	10	10	15	15	15	20	20	20

Table 9-5. The deposition conditions of the ZrO_2 films prepared at different total sputtering pressures

No. of the samples	Z10	Z11	Z12	Z13	Z14	Z15
Sputtering pressure (mbar)	1.5×10^{-2}	8×10^{-3}	6×10^{-3}	4×10^{-3}	2×10^{-3}	9×10^{-4}
P_{O2}	40%					
dc power (W)	85					
Substrate-target distance (mm)	60					
Substrate Temperature	Room temperature					
Sputtering time (Min.)	10	10	10	20	20	20

Table 9-6. The deposition conditions of the ZrO_2 films prepared at different substrate temperatures

No. of the samples	Z16	Z17	Z18	Z19	Z20
Substrate temperature (^oC)	25	200	300	350	400
Sputtering pressure (mbar)	5×10^{-3}				
P_{O2}	40%				
dc power (W)	90				
Substrate-target distance (mm)	60				
Sputtering time (Min.)	18	18	15	15	15

Table 9-7. The deposition conditions of the ZrO_2 films prepared at different substrate-target distances

No. of the samples	Z21	Z22	Z23	Z24
Substrate-target distance(mm)	60	65	70	75
Sputtering pressure (mbar)	5×10^{-3}			
P_{O2}	50%			
dc power (W)	90			
Substrate Temperature	Room temperature			
Sputtering time (Min.)	15	15	15	15

9.4.4. Multilayer films

The prepared multi-layers for fabricating ECDs are listed in Table 9-8, Table 9-9 and Table 9-10. In order to determine the thickness and morphology of the multilayers, Laser integral micro-topographic (LIMT) inspection was used. LIMT (MICROTOP.06.MFC) setup is shown in Fig.9-6 [32]. It has an active optical triangulation sensor and is performed in a non-destructive, non-invasive way. Its depth resolution can reaches 3 nm and lateral resolution is 1 μm.

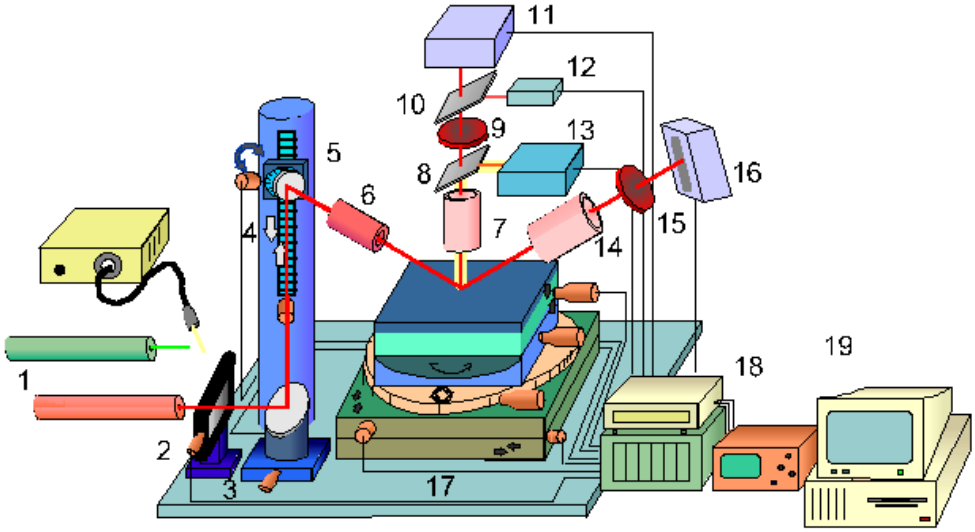

Note:

1. Interchangeable light sources; 2. Vibration isolation stand; 3. Neutral density filter;
4. Beam steering system; 5. Incidence angle control motorized system;
6. Incidence optics; 7. Normal observation optics; 8. and 9. Beam splitters;
10. Interference filter; 11. Normal photosensitive detection system; 12. Photodetector;
13. Video camera and illuminator; 14. Specular observation optics;
15. Interference filter; 16. Specular photosensitive detection system
17. Sample support and motorised positioning system;
18. Data acquisition and control system; 19. Microcomputer.

Fig. 9-6. Setup of the Laser integral microtopographic (LIMT, The MICROTOP.06.MFC) inspection.

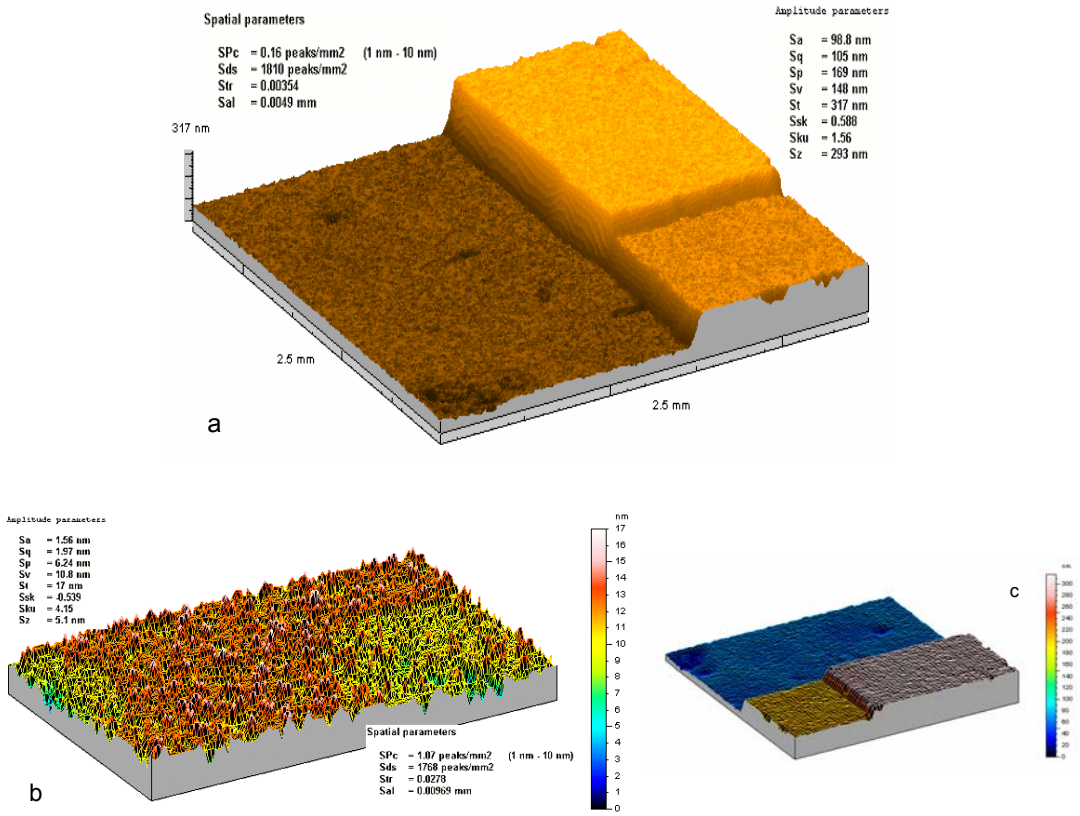

Fig. 9-7. Photograph of thickness and surface of the multi-layer film determined by the laser triangulation based microtopographer (LTBM). (a) WO_3/ITO/glass substrate from top to bottom; (b) Surface of WO_3 film, S_a= R_a, S_q= RMS (total roughness), S_{sk} = R_{sk}, S_t= total height difference; (c) Another angle observation of the multi-layer film.

In fact originally the LIMT was normally used to check the surface of the bulk material, opaque film and its surface. For measuring the transparent multilayer, we used the following proposed processes before measuring it. 1. Making a step type of the multilayer (Fig. 9-7a). 2. Making a cover reflection coating on the step area of the multilayer. It is called two pre-treatment processes or "step-semi-coating" method. After the two pre-treatment processes we can obtain the clear photographs of the bi-layer film (WO_3/ITO/glass substrate) like in Fig. 9-7.

In LIMT the skewness (S_{sk}) parameter gives information about the symmetry of irregularities perpendicular to the surface. In the WO_3 film [Fig. 9-7(b)] the irregularities have a good symmetry because the S_{sk} values are very small (0.539). The symmetry in the coating plane is also good because the kurtosis (S_{ku}) values are 4.15 (approximately 3) [33]. The total roughness (S_q= rms =R_q, see Section 3.8) is 1.97 nm. The total height difference (S_t) is less than 17 nm.

The correlation distance is one of the most important parameters measured. It gives us an indication of the lateral spacing of the surface irregularities. It is possible to conclude that the coating surface irregularities have a normal distribution. This distribution means that picks and vales on the surface are equally distributed.

From the photograph of the bi-layer film (WO_3/ITO/glass substrate) in Fig. 9-7, the top layer is WO_3 (~110 nm thickness), the middle layer is ITO (~200 nm thickness) and bottom layer is the glass substrate. The photograph shows the uniformity of the film surfaces. The developed LIMT can monitor thickness and surface of the multi-layer films conveniently. Similarly the thickness of ZrO_2 or SnO_2 films was also measured, while it is deposited on another ITO film.

Table 9-8. Layer structure and layer thickness of the samples

No. of the samples	A1	A2	A3	A4	A5
Structure	ITO/W O_3 (W2, P_{O2}: 70%)	ITO(d3)/W O_3 (W2, P_{O2}: 70%)	ITO(d3)/W O_3 (W3, P_{O2}: 60%)	ITO(d3)/W O_3 (WM2, P_{O2}: 70%; Mo: 5.0%)	ITO(d3)/W O_3 (WM5, P_{O2}: 60%; Mo: 5.0%)
Thickness (nm)	320/456	282/456	282/516	282/465	282/522
Number of layer	1/1	1/1	1/1	1/1	1/1

C: commercial product; h: Home made; T_s: Substrate temperature; T_a: Post annealing temperature, bracket: name of sample.

Table 9-9. Layer structure and layer thickness of the samples

No. of the samples	B1	B2	B3	B4	B5
Structure	ITO(d3)/W O_3 (WM6, P_{O2}: 60%; Mo: 3.8%)	ITO(c)/W O_3 (WM1, P_{O2}: 70%; Mo: 6.0%)	ITO(c)/W O_3 (WM4, P_{O2}: 70%; Mo: 1.9%)	ITO(d3)/W O_3 (WM1, P_{O2}: 70%; Mo: 6.0%)	ITO(c)/W O_3 (WM3, P_{O2}: 70%; Mo: 3.8%)
Thickness(nm)	282/518	320/465	320/456	282/290	320/456
Number of layer	1/1	1/1	1/1	1/1	1/1

Table 9-10. Layer structure and layer thickness of the samples

No. of the samples	O1	O2	O3	O4	O5
Structure	ZrO_2 (Z16, P_{O2}: 40%) / ITO(c)	SnO_2 (H4, P_{O2}: 30%, plus T_s: 250 ^{0}C) / ITO(d3, plus T_a: 300 ^{0}C)	ZrO_2 (Z20, P_{O2}: 40%, T_s: 400 ^{0}C) / ITO (d3)	SnO_2 (H9, P_{O2}: 30%, plus Ts: 400 ^{0}C, Fe: 1.5%) / ITO(d3)	SnO_2 (H4 plus T_s: 250 ^{0}C) / ITO(d3, plus T_a: 300 ^{0}C)
Thickness(nm)	160/320	240/289	180/282	200/282	240/289
Number of layer	1/1	1/1	1/1	2/1	1/1

9.4.5. Different configurations and operation of EC devices

a. Multi-layer configuration with two pieces of glasses

After putting the Li^+ solid state electrolyte between the "glass / ITO /WO_3 " and the "ZrO_2 (or SnO_2)/ ITO / glass", the fabrication of one EC window was finished. Li^+ solid electrolyte can be an of inorganic compound, hybrid of inorganic and polymer material. It can be deposited using vacuum vapor deposition, solution drop and dip-coating techniques on WO_3 and counter-electrode films. Both electrodes are firmly pressed together to assure a good mechanical and electrical contact in the fabrication of ECDs. Many different kinds of configurations of ECDs are fabricated. They are "A1 (Table 9-8)/ Li^+ solid state electrolyte /O1(Table 9-10)(device F1)", "A2/ Li^+ solid state electrolyte /O2(device F2)", " B1/ Li^+ solid state electrolyte /O3(device D3)", "B2/ Li^+ solid state electrolyte /O4(device D4)", "B3/ Li^+ solid state electrolyte /O5(device D5)", and so on from Table 9-8, Table 9-9 and Table 9-10. The photographs of the operation of the actual ECDs are presented in Fig. 9-8. The left photo in Fig. 9-8(a) shows that 5 volts voltage is just being applied to the device F1. The right photo shows that the coloring state of device F1 after 5 volts was applied for 2 seconds. Fig. 9-8(b) and (c) shows the operation of the device D4. They are found to exhibit a considerable reduction of the transmittance in the visible range, stability and reversibility in electrochromic properties. They can withstand more than a few hundreds of coloration-bleaching cycles and have an open-circuit memory of more than five days.

b. Multilayer configurations with one piece of glass

The EC devices on one piece of glass were fabricated by the composition based on multilayers presented in Table 9-8 and Table 9-9. For example, Li^+ solid state electrolyte, SnO_2 (or ZrO_2), ITO can be deposited on the sample forming layer A_n (or B_n, n=1, 2, 3, 4, 5) and finally formed the EC devices with only one piece of glass.

c. The observed modulation in transparent spectra

During operation of the device lithium ions were intercalated electrochemically into the WO_3 film. The optical transmittances of F1 and D4 devices were measured in the wavelength range 300 nm to 3200 nm for both coloring and bleaching states (Fig.9-9 a, b).

The two devices were colored by the application of a 5 V dc voltage. In Fig. 9-9 (a) the transmission spectra of a typical EC device (F1) incorporating a WO_3 film are shown. The device has 84% maximum transmittance (T_{max}) in the as-prepared state. A 68% decrease in T_{max} can be observed after coloration (with the application of 5 V for 2 seconds). This kind of performance is considered satisfactory for future commercial EC devices or EC windows. The device exhibits significant open circuit memory. The dark color can be kept for five days after coloration. The coloration-bleaching cycle of the device is fully reversible. The solid line of the curve is the transmittance spectrum of the device without glass substrate (or deducting the substrate effect).

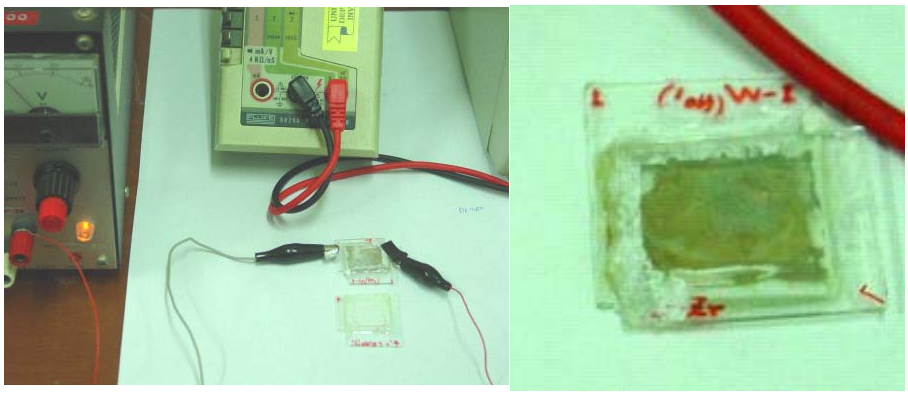

Device F1 at 1 second Device F1 after 2 seconds

Fig.9-8 (a). The operation of a prototype electrochromic (EC) window (Device F1).

In device D4, the maximum change of the transmittance is up to 30% in the visible range after Li intercalation in the WO_3 film (Fig. 9-9 b). The shift of the absorption peak is interpreted as an increase in the Fermi level of the material as more Li ions are inserted. The optical transmittance of the devices F2, D3, and D5 was measured in the

wavelength range 300 nm to 3200 nm with and without glass substrate (Fig.9-10 a, b, c). It is clearly seen that two pieces of glass on the device have an effect at least 20% to the transmittance of the device. The real multilayer without glass exhibited a maximum of 97 % transmittance in the bleached state.

It can be inferred from the experiments, that ECDs can exhibit higher coloration efficiency, if they have an ion storage layer. They exhibit higher speed of colouration, as they have an ion storage layer made of Fe doped SnO_2. It therefore becomes evident that the use of ion storage layers can improve the performance of EC devices.

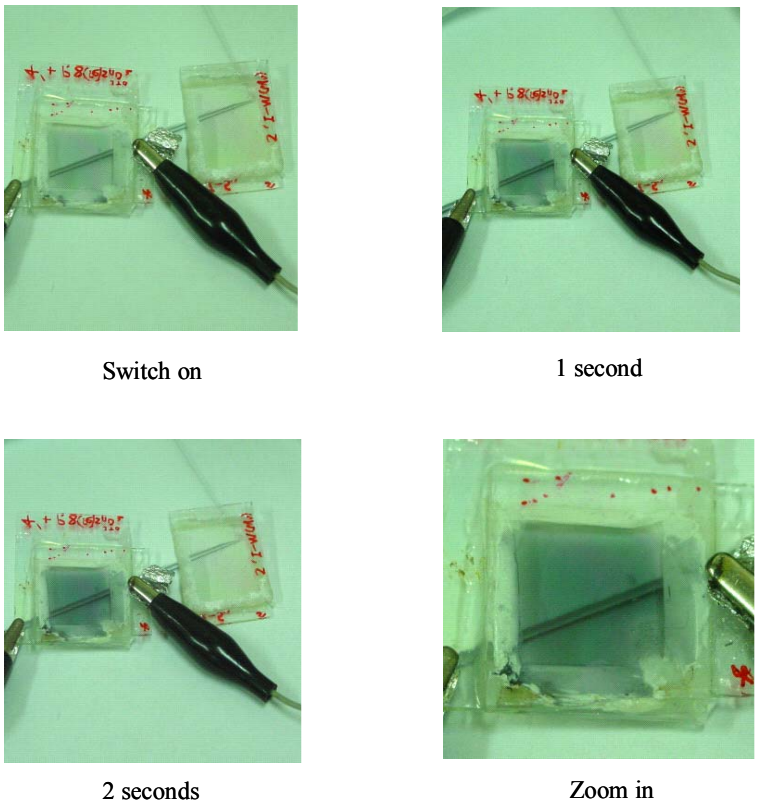

Fig.9-8 (b). The operation of an electrochromic (EC) window device (D4).

Fig. 9-8 (c). Picture of the operation of device D4.

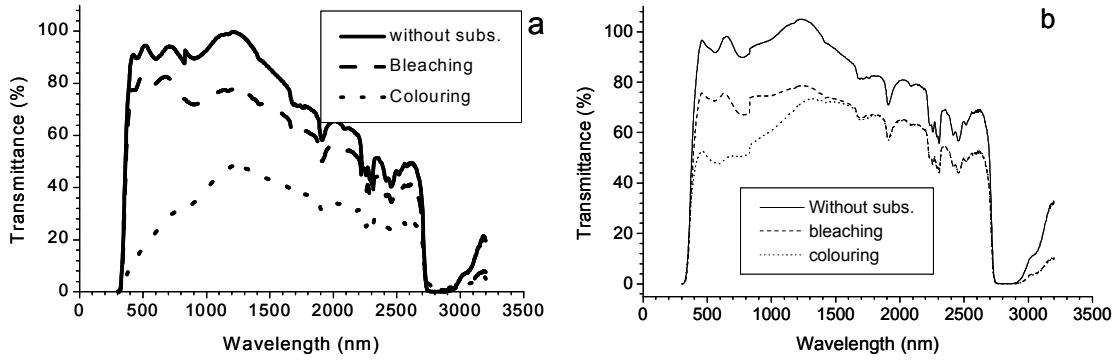

Fig. 9-9. The optical transmittances were measured for coloring and bleaching states, (a) device F1, (b) device D4.

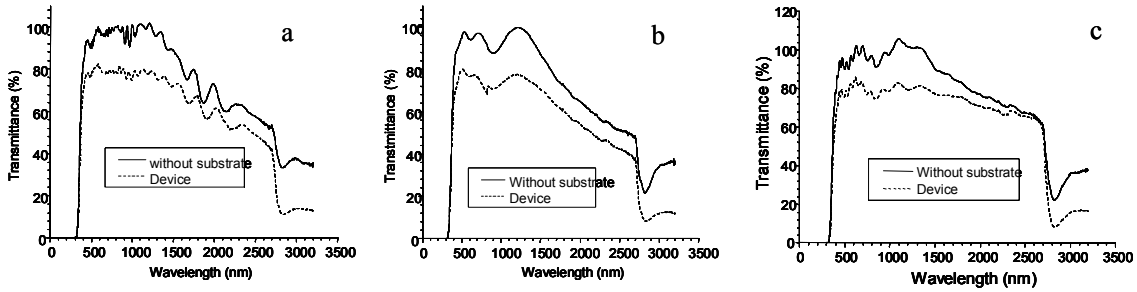

Fig. 9-10. The optical transmittances of the multilayers were measured with and without glass substrate, (a) device F2, (b) device D3, (c) device D5.

9.5. Summary of the Chapter

The structure of the EC film strongly influences the EC properties. In the study of the films, the structural models based on hexagonal WO_3, in which three- and six-membered rings of octahedra are present. They were discussed for ionic conduction. The structure of the WO_3 films decided mainly if the film can exhibit suitable kinetic behavior for different kinds of ions insertion/extraction. The tunnel data of ion transition in different structures of the film is deduced and given. For crystalline and amorphous WO_3, the theoretical and structural pictures give us the explanation on elecotrochromism. The fast coloration/bleaching dynamical process is dominated by the tunnel size of crystalline structure of the WO_3 film and relative size of the ions, and not only the porosity of the film as in the traditional opinion. A forced intercalation model

was proposed. It can explain some EC phenomenon such as the no reversibility and changing of the diffusion constant κ_d.

In this chapter it was also developed a simulation model for charge injection in electrochromic films. A differential equation of the mathematical physics involved was hypothesized and discussed. Application of the model to the coloration of electrochromic devices is discussed in two particular cases.

SnO_2 and ZrO_2 counter electrodes or ion storage layers (IS) were prepared for electrochromic devices. These materials were incorporated into electrochromic devices. The LIMT inspection was developed to evaluate a transparent multilayer and its cross section. The two pre-treatment processes (or "step-semi-coating") method before measurement was proposed. After the processes we can obtain clear photographs of the transparent films.

The configuration of the smart EC devices (ECDs) is: ITO (Indium-tin-oxide)/WO_3/Li^+-electrolyte/counter electrode film/ITO. Depending on the choice of different counter electrodes such as SnO_2, V_2O_5, ZrO_2 and the relevant Mo (or Fe) doped films, a total of 16 window structures were fabricated and studied. The window composed by a multilayer between two pieces of glass exhibited a maximum optical transmittance of 84 % and a minimum of 16% before and after applying 5 V for 2 seconds (or in bleached and coloured state). The real multilayer without glass exhibited a maximum of 97 % transmittance in the bleached state. The tested devices can withstand more than a few hundreds of coloration–bleaching cycles and have an open-circuit memory of more than five days. They are suitable for EC glazing, switching devices and other applications.

9.6. References

[1] A. Temmink, O. Anderson, K. Bange, H. Hantsche, X. Yu, Thin Solid Films 192 (1990) 211

[2] J. V. Gabrusenoks, P. D. Chikmach, A. R. Lusis, J. J. Kleperis, G. M. Ramans, Solid State Ion, 14 (1984) 25

[3] S. K. Deb, Phil. Mag. 22 (1973) 801.

[4] Chemistry: WebElements Periodic Table: Professional Edition: Hydrogen: radii- http://www.webelements.com/webelements/elements/text/H/radii.html.

[5] C. G.Granqvist, Eelectrochromic Materials: Microstructure, Electronic Bands, and Optical Properties, Applied Physics A-Solids and Surfaces, 57 (1993) 3-12.

[6] C. G. Granqvist, Handbook of Inorganic Electrochromic Materials, (Elsevier, Amsterdam, 1995).

[7] L. S. Wang, B. P. Hichwa, S. P. Sapers, J. G. H. Mathew, N. A. O´Brien, in: J. B. Bates (Ed.), Proc. Symp. Thin Film Solid State Ionic Devices and Materials, Proc. Vol. 95-22, The Electrochem. Soc. Pennington, 1995, pp. 63-75.

[8] M. Stromme Mattsson, Phys. Rev. B 58 (1998) 11015.

[9] H. Bach, D. Kraus (Eds.), Thin Films on Glass, Springer-Verlag (Berlin, Germany) 1997, p.195

[10] B.W. Faughnan, R.S. Crandall, Electrochromic Display Based on WO_3, in: Topics in Applied Physics, vol. 40, Display Devices, J.I. Pankove, (Ed.), Springer, Berlin, (1980), ch. 5.

[11] Z. Luo, Z. Ding, Z. Jiang, J. Non-Cryst. Solids. 112 (1989) 309.

[12] B. Vuillemin, O. Bohnke, Solid State Ionics 68 (1994) 257.

[13] O. Bohnke, M. Rezrazi, B. Vuillemin, C. Bohnke, P.A. Gillet, Solar Energy Mater. Solar Cells 25 (1992) 361.

[14] J. Hladik (Ed.) Physics of Electrolytes, Volume 1, Transport Processes in Solid Electrolytes and in Electrodes, Academic Press, London.1972

[15] N. S. Koshlyakov, M. M. Smirnov, E. B. Gliner, Differential Equations of Mathematical Physics, North-Holland Publishing Company, Amsterdam, 1964, P118

[16] G. Leftheriotis, S. Papaefthimiou, P.Yianoulis, Sol. Energy Mater. Sol. Cells 61 (2000) 107.

[17] R. Lechner, L. K. Thomas, Sol. Energy Mater. Sol. Cells, 54 (1998) 139.

[18] I. Porqueras, E. Bertran, Thin Solid Films 377-378 (2000) 8.

[19] I. Porqueras, E. Bertran, Thin Solid Films 377-378 (2000) 129.

[20] Z. M. Jarzebski and J. P. Marton, J. Electrochem. Soc., 123 (1976) 199C, 299C, 333C.

[21] J. M. Correia-Pires, J. B. Almeida, V. Teixeira, "Gas sensitive response of SnO_2 thin film sensors produced by reactive DC magnetron sputtering", Key Engineering Materials 230-232 (2002) p.388-391

[22] C. G. Fonstad, A. Linz and R. H. Rediker, J. Electrochem. Soc., 116 (1969) 1269

[23] J. Miguel Correia-Pires, Vasco Teixeira, J. Borges de Almeida, "Deposition of SnO2-based thin films by reactive DC magnetron sputtering for gas sensing applications", Nanostructured Materials and Coatings for Biomedical and Sensor Applications, Kluwer Academic Publishers, Ed. Y.G. Gogotsi and I.V. Uvarova, (2003), p. 343-355

[24] W. Tang and D.C. Cameron, Thin Solid Films, 238 (1994) 83

[25] J. Gottmann, A. Husman, T Klotzbucher, E.W. Kreutz, Surf. Coating Technol. 100 (1998) 411

[26] Vasco Teixeira, Martin Andritschky, High Temp.-High Pressures 25 (1993) 213

[27] A. Portinha, V. Teixeira, J. Carneiro, M. F. Costa, N. P. Barradas and A. D. Sequeira, "Stabilization of ZrO_2 PVD coatings with Gd_2O_3", Surface and Coatings Technology, 188-189 (2004), 107-115.

[28] V. Teixeira, M. Andritschky, W. Fischer, H. P. Buchkremer, and D. Stover, Surf. Coatings Technl., 120 (1999) 103

[29] D. K. Fork, A. Barrera, T. H. Geballe, A. M. Viano, and D. B. Fenner, Appl. Phys. Lett., 57 (1990) 2504

[30] G. L. Tan, and X. J. Wu, Thin Solid Films, 330 (1998) 59

[31] R. D. Maggio, L. Fedrizzi, S. Rossi, and P. Scardi, Thin solid Films, 286 (1996) 127

[32] Costa Manuel F. M. Proc. Soc. Photo. Instrum. Eng. 4087 (2001) 1214.

[33] M. F. M. Costa and J. B. Almeida, "System of optical noncontact microtopography," Appl. Opt. **32**(25), pp. 4860-4863, 1993.

Conclusion of the thesis

In this thesis, we have focused on the study of the influence of the deposition conditions and Mo (or Fe) doping on the microstructure and the properties of the films (ITO, WO_3, SnO_2, V_2O_5 and ZrO_2). The functional films such as transparent conduction film, thermochromic (TC) film and thermotropic (TT) film, Bi-layer CdS/ITO, and multi-layer films based on WO_3 were also systematically investigated. Relevant theories, experiments and technique discussions were done to obtain the optimized electrochromic (EC) device. Briefly, the following conclusions were obtained.

1. We successfully designed and fabricated a solid electrochromic device (ECD) using a magnetron sputtering technique. A maximum modulation of 68% was obtained at an optimal case after coloration (applied 5 V for 2 seconds). The real multilayer without glass substrate exhibited a maximum of 97 % transmittance in the bleached state.
2. It can be inferred from the experiments, that ECDs can exhibit higher coloration efficiency, if they have an ion storage layer. They exhibit higher speed of colouration, as they have an ion storage layer made of Fe doped SnO_2. It therefore becomes evident that the use of ion storage layers can improve the performance of EC devices.
3. We successfully designed and fabricated transparent conduction ITO (Indium-tin-oxide) films and CdS/ITO bi-layers by a modified dc sputtering method. The prepared ITO films yield the lowest sheet resistance (R_s) of 26.5 Ω/Sq and highest transmission of 94% by using a ceramic target. Depending on the application, both amorphous and polycrystalline ITO films are obtained by controlling the deposition conditions. They can be used in many fields such as photo-electronics, energy engineering, industry and consumer goods.
4. A simulation model of ECDs for charge injection and extraction was developed. A differential equation was hypothesized and discussed in term of physics. The model was analyzed in a particular case for the coloration state of the EC devices.

5. The formation and configuration of the structural model based on hexagonal WO_3, in which three- and six-membered rings of octahedra are displayed, were introduced and developed. They exhibit suitable kinetic behaviour of ions insertion / extraction for ECDs. A forced intercalation model was proposed. It can explain some EC phenomenon such as no reversibility, and can give a strong effect to the normal diffusion constant κ_d. The fast coloration/bleaching dynamical process is explained. It is because of the film crystalline structure that suits certain ion size and not only the porosity of the film as in the traditional explanations.
6. The LIMT (Laser integral micro-topographic) inspection was developed to evaluate a transparent multilayer and its cross section. The two pre-treatment processes or or "step-semi-coating" method before measurement was proposed. After the processes we can obtain the clear photographs of the thin transparent films.
7. Total integrated scattering (TIS or spectra calculation) was introduced to evaluate roughness (δ) of the film surface. A minimum roughness value of the surface of ITO films, which was obtained at RT, is 8.0 nm. The film surface becomes rougher up to 14.0 nm as T_a is increased. The results are in good agreement with SEM, AFM, AFM statistical analysis and other methods.
8. The refractive index (n), the extinction coefficient (κ) and energy band gap (E_g) were derived, analysed and obtained from the measured spectra using physical models such as the Swanepoel model (Section 3.6), the Scattering model (Section 5.2), the direct transition semiconductor model (Section 3.7). The calculation equation of optical parameter- extinction coefficient (κ) was obtained by diffuse reflectance spectrum method using "scattering model". Clearly the results of the "scattering model" and Ellipsometric method agree in magnitude. The thin thickness of the film can cause the increasing of substrate effect and makes high E_g. The thinner the film is, the higher the optical band gap is. The E_g value varies in range of 3.26 eV-3.88 eV for different ITO films. All these measurements are important to evaluate the deposited films for real applications.
9. The equations for the dielectric function and photo energy were derived using a theoretical physical model (Drude theory, Section 5.3). The expressions and calculations of the electric charge density (n_c) and the carrier mobility (μ) from

the optical parameters were given by using Mathematica-4.1 software. The electrical characteristics n_c and μ were compared and studied by experimental measurements and calculations using Mathematic-4.1 software. Both measured and calculated values coincide in magnitude. For the ITO sample h4 the experimental values of n_c and μ are 4.18×10^{20}(cm^{-3}) and 11.80(cm^2/V•s). The calculated value of n_c and μ is 1.54×10^{21} (cm^{-3}) and 1.21 (cm^2/V•s) at 540 nm ($\omega = 2\pi\nu = 2\pi C/\lambda = 3.47 \times 10^{15}$ S^{-1}, C is the speed of light). The calculated n= 1.89, κ=0.17, $\omega_\rho = 4.04 \times 10^{15}$ m^{-1} and $\omega_\gamma = 4.85 \times 10^{15}$ m^{-1} were obtained by using the Mathematica-4.1 Software.

10. The WO_3 and V_2O_5 thin films on a glass substrate were successful analyzed in the infrared (IR) in the ECDs study, using IR reflective absorption in near grazing incidence angle (NGIA) technique. Due to IR high sensitivity to the presence of the OH group, direct experimental proof of the presence of water in the films was obtained from the IR spectrum. A broad band in the 3250-3600 cm^{-1} region, and two peaks located at 1613 cm^{-1} and 1453 cm^{-1} were studied. Those bands originate from moisture and are assigned to ν(OH) and δ(OH) modes of adsorbed water. This is important due to the role-played by water in the EC mechanism.
11. Molecular vibration spectra were proposed to distinguish the phase and structure of these inorganic thin films. It was found that Raman plus IR spectroscopy, is a powerful technique to investigate EC films. Comparing our Raman spectra with that of polycrystalline WO_3 and α-WO_3 films, our WO_3 films have both polycrystalline WO_3 (in the range 100-300 cm^{-1}) and α-WO_3 (in the range 500-1000 cm^{-1}), but mainly the α-WO_3 phase. Further Raman curve fitting analysis was done and confirmed that the prepared films are composed by WO_3. It is found that the spectrum of the annealed WO_3 film is characterized by as many as 7 modes in the 600 - 1000 cm^{-1} region.
12. All the studies of the V_2O_5 films indicate that the V_2O_5 films are good TC (thermochromic) and TT (thermotropic) materials. The films exhibit clear changes in transmittance when the temperature is varied, specially in the 3600-4000 cm^{-1} range. After applying higher T ($>T_c$), the films have a good transmittance variation. The maxmium variation of transmittance reaches 49% at 4000 cm^{-1}. The films exhibit good changes in resistance in the RT-350 ^{0}C range. The maximum change of R_{2p}/T can reach 1200 $\Omega/^0$C. There is tendency of

bigger variation of transmittance when the Mo doping ratio of the film or the P_{O2} of the film is larger, after applying temperature of 200 ^{0}C to the samples.

13. In the study of bi-layer CdS/ITO, the CdS film was grown through the USCD (ultrasonic colloid deposition) method. It can produce bar-shaped ultra fine particle films of cadmium sulfide via a simple, low cost process. The formation mechanism of the bar-shaped structure of CdS, plus other bar-shaped structures of ITO and V_2O_5 films were discussed using the three important models of thin film growth (Volmer-Weber, van der Merwe, and Stranski-Krastanov mechanism) presented in Chapter 6.
14. Our studies on the preparation and characterization of the films offer detailed data and references to further research work and industrial production.

Apendix I

List of the tables of sample names for electrochromic devices

ITO samples

WO_3 samples

V_2O_5 samples

SnO_2 samples

ZrO_2 samples